Journal of Hazardous Materials 166 (2009) 39–45

Contents lists available at ScienceDirect

Journal of Hazardous Materials

journal homepage: www.elsevier.com/locate/jhazmat

Quantifying effects of pH and surface loading on arsenic adsorption on NanoActive alumina using a speciation-based model

Xiao-Hong Guan[a,b], Tingzhi Su[b,c], Jianmin Wang[b,*]

[a] School of Municipal and Environmental Engineering, Harbin Institute of Technology, Harbin, PR China
[b] Department of Civil, Architectural & Environmental Engineering, Missouri University of Science and Technology, 1870 Miner Circle, Rolla, MO 65409, USA
[c] College of Environmental Science and Engineering, Tongji University, Shanghai, PR China

ARTICLE INFO

Article history:
Received 10 July 2008
Received in revised form 29 October 2008
Accepted 31 October 2008
Available online 7 November 2008

Keywords:
Arsenic
Alumina
Adsorption
FTIR
Speciation-based model

ABSTRACT

Arsenic (As) poses a significant water quality problem and challenge for the environmental engineers and scientists throughout the world. Batch tests were carried out in this study to investigate the adsorption of As(V) on NanoActive alumina. The arsenate adsorption envelopes on NanoActive alumina exhibited broad adsorption maxima when the initial As(V) loading was less than a 50 mg g^{-1} sorbent. As the initial As(V) loading increased to 50 mg g^{-1} sorbent, a distinct adsorption maximum was observed at pH 3.2–4.6. FTIR spectra revealed that only monodentate complexes were formed upon the adsorption of arsenate on NanoActive alumina over the entire pH range and arsenic loading conditions examined in this study. A speciation-based adsorption model was developed to describe arsenate adsorption on NanoActive alumina and it could simulate arsenate adsorption very well in a broad pH range of 1–10, and a wide arsenic loading range of 0.5–50 mg g^{-1} adsorbent. Only four adjustable parameters, including three adsorption constants, were included in this model. This model offers a substantial improvement over existing models in accuracy and simplification in quantifying pH and surface loading effects on arsenic adsorption.

© 2008 Elsevier B.V. All rights reserved.

1. Introduction

Inorganic species of arsenic (As) represent a potential threat to the environment, human health, and animal health due to their carcinogenic and many other effects. Several diseases, including a number of different types of cancers, have been linked to the consumption of arsenic-containing groundwater in Bangladesh, Taiwan, Argentina, Mexico, Chile, China, Hungary, Thailand, USA, New Zealand, South Africa, and India [1–3]. Consumption of arsenic also leads to disturbance of the cardiovascular and nervous system functions and eventually leads to death [4]. In order to reduce arsenic exposure through drinking water consumption, the United States Environmental Protection Agency (U.S. EPA), the World Health Organization (WHO) and the Ministry of Health of the People's Republic of China have lowered their regulatory or guideline values for total As concentration in drinking water to 10 μg l^{-1}.

Several treatment methods have been developed for the removal of arsenic from water, including flotation [5], precipitation with sulfide [6], coagulation [7], ion-exchange, and desalting techniques such as reverse osmosis or electrodialysis [8]. These methods may not be feasible for point-of-use (POU) applications due to the requirement for continuous attention during the treatment. Some of them may produce large amounts of chemical sludge which needs further treatment before being disposed of [4]. As an alternative to these treatment methods, adsorption has been recognized as an effective technique for removing arsenic. Therefore, accurate prediction of arsenic adsorption for different field water quality conditions is needed in order to properly design and operate the treatment system.

A commonly used approach for modeling arsenic adsorption considers surface electrostatic effects. These models include constant capacitance model [9–12], diffuse layer model [13,14], triple layer model [10,15,16], generalized two-layer model [17], and CD-MUSIC model [18–20]. These models incorporate the surface electrostatic effects on the adsorption calculation. Venema et al. [21] discussed the scope and limitations of five such models and commented that, while most of these models can satisfactorily quantify the adsorption phenomenon, none of them can simultaneously describe all available data for a particular extended data set. Moreover, consideration of the surface electrostatic effects in these models makes the modeling process very complex, which limits their practical application. Therefore, a robust model that is capable of predicting arsenic adsorption under various field water quality conditions, especially the pH and arsenic concentration, is needed. Such a model could be used to determine the proper unit size for column treatment systems and the operation time (before

* Corresponding author. Tel.: +1 573 341 7503; fax: +1 573 341 4729.
E-mail address: wangjia@mst.edu (J. Wang).

0304-3894/$ – see front matter © 2008 Elsevier B.V. All rights reserved.
doi:10.1016/j.jhazmat.2008.10.121

saturation of the column) based on the field water quality conditions.

Activated alumina adsorption is considered to be inexpensive and convenient to use [22,23] due to its strong selectivity to arsenate ion [24], especially for POU applications [24–26]. NanoActive alumina is a commercial alumina that is produced using proprietary processes to obtain an amorphous material with a large specific surface area and low density that has high adsorption capacity and chemical reactivity. This study examined the adsorption performance of As(V) on NanoActive alumina to validate a robust, speciation-based model that would simulate arsenate adsorption under various pH and surface loading conditions. Such a model has the potential to be used for the prediction of arsenic adsorption capacity of column systems, therefore is important for treatment system design and operation based on local water quality conditions.

2. Materials and methods

Reagent-grade chemicals and de-ionized (DI) water were used to prepare all solutions. NanoActive alumina, with the mean aggregate size of 1.5 μm and the BET area of 359 $m^2\,g^{-1}$ was purchased from NanoScale Materials, Inc., Manhattan, KS.

2.1. Batch equilibrium titration

A batch equilibrium titration method was employed to determine the surface site density and acidity constant of NanoActive alumina. The titration procedure consisted of: (a) distributing a certain amount of sorbent and 100 ml of DI water containing 0.1 M $NaNO_3$ to each of a series of 125 ml HDPE plastic bottles; (b) adding different amounts of standard acid or base stock solution to these bottles to adjust the pH to a range of 1–13; keeping one unit without adding acid or base as the control; (c) sealing up all bottles and shaking them at 180 oscillation min^{-1} using an EBERBACH 6010 shaker for 24 h; (d) measuring the final pH, and plotting the acid/base addition volume as a function of pH to obtain an overall titration curve; (e) filtrating the suspensions and titrating the filtrate back to the pH of the control; (f) developing a net titration curve by subtracting the acid/base consumed by the filtrate from the overall titration curve; and (g) modeling the net titration data using a non-linear regression program, NLREG (P.H. Sherrod, Brentwood, TN). An Orion pH meter (perpHecT LoR model 370) with an Orion PerpHecT Triode pH electrode (model 9207BN) was used to measure pH.

2.2. As(V) adsorption experiment

The batch equilibrium experiments to determine arsenate adsorption on NanoActive alumina were conducted at a pH ranging from 1 to 13, with initial arsenic concentrations ranging from 5 to 500 mg l^{-1}, and a sorbent concentration of 10 g l^{-1}. The broad pH range was selected to induce the protonation and deprotonation reactions of different surface sites. Theoretically, the broad arsenic concentration range was selected to evaluate the adsorption behavior of arsenate in different regions of the sorption isotherm, that is, (i) the initial proportional adsorption region, (ii) the intermediate region, and (iii) the maximum adsorption region. In addition, the ultimate goal of this research was to determine adsorption constants to be used for the prediction of column adsorption capacity, based on field water quality (pH and influent arsenic concentration). In adsorption columns, the sorbent continually accumulate arsenic. The saturated section of the column, i.e., the section prior to the mass transfer zone, is in equilibrium with the influent arsenic concentration. Therefore, the total column capacity (i.e., the total adsorbed arsenic) needs to be estimated using the influent arsenic concentration as the equilibrium concentration. When a batch experiment is conducted to determine adsorption constants appropriate for column capacity prediction, an arsenic loading consistent with that for the saturated section of the column, i.e., the section prior to the mass transfer zone, needs to be used. With this loading, the equilibrium arsenic concentration in solution after adsorption should be equal to that normally seen in raw water (parts per billion level). As a result, the total (i.e., initial) arsenic concentration used for batch experiments should be significantly greater than that found in raw water, depending on the sorbent concentration. It has been reported that the As content of residual sludges from arsenic removal systems can be in a range of 1–10 mg g^{-1} [27,28]. Therefore, for a batch system with a sorbent concentration of 10 g l^{-1}, the total arsenic concentration should be slightly in excess of 10–100 mg l^{-1}. Considering some extreme arsenic concentration conditions, and the presence of other competing elements in the raw water, a broader arsenic concentration range of 5–500 mg l^{-1} was used in this study. A broader arsenic loading range also allowed us to examine the arsenic adsorption behavior and validity of the model under near saturation conditions.

A 100 ml solution containing 0.1 M $NaNO_3$ and the pre-selected concentration of As(V) were added to each of a series of 125 ml HDPE plastic bottles containing a pre-selected amount of sorbent. The pH of the mixture was then adjusted using stock HNO_3 or NaOH solutions. All flasks were then sealed and shaken for 24 h. As a standard practice, duplicate samples and sample blanks are used in our batch experiments for QA/QC purposes.

2.3. Chemical analysis

At the end of each adsorption test, the suspensions were immediately filtered through a 0.45-μm membrane filter made of cellulose acetate (MFS) and the filtrates were collected for the arsenate analyses. A graphite furnace atomic absorption spectrometer (AAnalyst 600, PerkinElmer Corp., Norwalk, Connecticut, USA) was used to determine arsenic concentrations in solution.

Electrophoretic mobility was used to determine the surface charge of alumina particles at various pH values and the point of zero charge (PZC) is the pH value that results in the value of the electrophoretic mobility being zero. Colloidal alumina particles were diluted in 100 ml of a 0.01 M $NaNO_3$ solution. The pH of the solution was adjusted either by NaOH and HNO_3 solution and was left to equilibrate for 1 day. The electrophoretic mobility of the alumina particles was observed at room temperature with a Zetasizer 3000HSA (Malvern Instruments Ltd., UK).

The SEM image of NanoActive alumina was collected with a Hitachi S-570 LaB6 SEM. XRD analysis was carried out with a Rigaku Miniflex Diffractometer to characterize NanoActive alumina. The BET specific surface area, pore volume, and pore size of NanoActive alumina were examined with a Quantachrome Autosorb-1-C high performance surface area and pore size analyzer.

Diffuse reflectance FTIR spectra of powdered samples were recorded on a Nexus 470 FT-IR (Thermo Electron Co.). The samples were diluted to a concentration of 2% with IR-grade KBr. Sixty-four co-added scans were collected at 2 cm^{-1} resolution in the mid-IR region (4000–400 cm^{-1}) for pure KBr and for each KBr-mixed sample. Vibrational spectra of each sample were obtained by subtracting the background spectra (pure KBr) from the spectra of a KBr-mixed sample. The ATR-FTIR spectra of aqueous arsenate at various pH levels were examined using attenuated total reflection Fourier Transform infrared spectroscopy. The ATR cell was equipped with a trapezoidalm ZnSe crystal (45° angle of incidence) as the internal reflection element. The ZnSe crystal was washed with deionized water at the end of each sample scan. To minimize oxoanion reactions with the ZnSe crystal, the spectra were

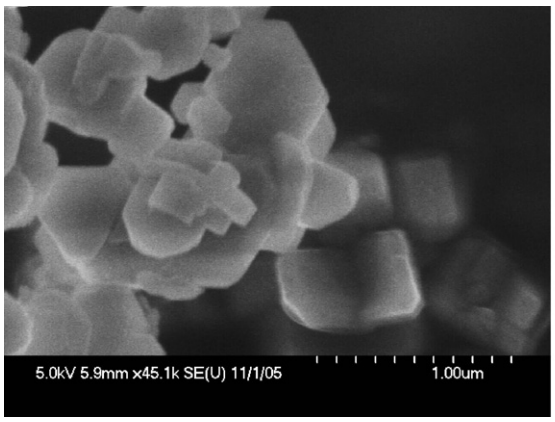

Specific surface Area (BET)	359 m^2 g^{-1}
Total pore volume	0.269 cm^3 g^{-1} (in pores less than 79.6 nm)
Average pore size	2.99 nm
Peak mesopore diameter	2.5 nm

Fig. 1. Scanning electron microscopy image and properties of NanoActive alumina.

immediately collected after the solutions were transferred into the ATR-cell. Background subtractions were made to remove bulk water spectra.

3. Results and discussion

3.1. Characterization of NanoActive alumina

Fig. 1 shows the SEM image and the physical properties of NanoActive alumina. It has a very smooth surface and XRD analysis revealed that NanoActive alumina is a typical Al_2O_3 (The XRD result is not shown). The NanoActive alumina particles were aggregated in solid state and could be dispersed in water with greatly reduced particle sizes. The BET surface area of the NanoActive alumina was 359 m^2 g^{-1} and the pore volume and average pore size were 0.269 cm^3 g^{-1} and 2.5 nm, respectively.

Zeta potential of NanoActive alumina was collected as a function of pH using 0.01 M $NaNO_3$ as the supporting electrolyte, as demonstrated in Fig. 2. Obviously NanoActive alumina carries a positive charge at pH below 8, while it is negatively charged at pH over 8.

3.2. Arsenate adsorption edges on NanoActive alumina

Arsenate speciation is pH dependent and H_3AsO_4, $H_2AsO_4^-$, $HAsO_4^{2-}$ and AsO_4^{3-} are the dominant species in the following pH ranges: <2.3, 2.3–6.8, 6.8–11.3, and >11.3–14, respectively

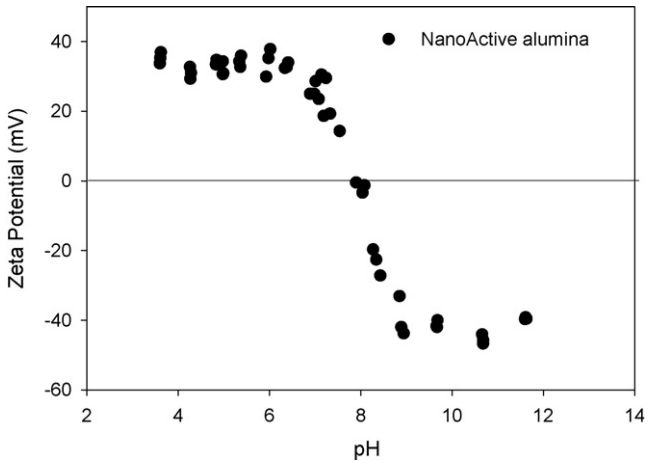

Fig. 2. Zeta potential of NanoActive alumina as a function of pH using 0.01 M $NaNO_3$ as the supporting electrolyte.

[29]. In addition, the surface charges of NanoActive alumina are pH dependent, as shown in Fig. 2. At pH values below the pH_{pzc} of the adsorbent, the surface of adsorbent particles is positively charged and vise versa. This indicates that surface site speciation changes with pH. Consequently, the adsorption of arsenate on NanoActive alumina is expected to depend on pH. The effect of pH on As(V) adsorption on NanoActive alumina was examined over a pH range of 1–13, with the initial As(V) concentration ranging from 5 to 500 mg l^{-1}, with the results presented in Fig. 3. The adsorption envelopes indicated that almost 100% of arsenate was adsorbed on NanoActive alumina throughout a pH range of 1.2–11, when the initial As(V) concentration was 5 or 10 mg l^{-1} (equivalent to 0.5 or 1.0 mg g^{-1} alumina). Results indicated that the adsorbed amount of arsenic was proportional to its initial concentration, i.e., the plots of As(V) adsorption ratio (the fraction of As(V) adsorbed on adsorbent) as a function of pH overlapped when the initial As(V) concentration were 5 and 10 mg l^{-1} (figures not shown), suggesting that the As(V) adsorption is in the linear range of Langmuir isotherm. Over 99.9% of arsenate was adsorbed at pH < 9.2, pH < 8.2, and pH < 7.9, when the initial As(V) concentrations were 50, 100, and 200 mg l^{-1}, respectively. However, arsenate adsorption on NanoActive alumina decreased significantly beyond these pH ranges, indicating that the adsorption edge of arsenate shifted to a lower pH level with increasing arsenate concentrations. As the initial As(V) concentration further increased to 500 mg l^{-1}, a distinct adsorption maximum at pH 4.0–4.6 was observed.

Some researchers found that almost 100% of arsenate was adsorbed by alumina at a pH below a certain value, which was related to the initial As(V) concentration, while arsenate adsorption decreased considerably with a further increase in pH [10,12,30], similar to the trends demonstrated in Fig. 3(b). This is because these researchers employed very low surface loading in their experiment. Other researchers observed that adsorption of arsenate decreased when the pH increased from the starting pH [31,32], which was ascribed to the narrow pH range (pH 4–9) employed in their studies.

The adsorption maximum for the initial As(V) concentration of 500 mg l^{-1} appeared in the pH range of 3.2–4.6, when $H_2AsO_4^-$ anions are the dominant species in the solution. The reduction in arsenate adsorption at excessively low pH may be associated with a reduction in the fraction of $H_2AsO_4^-$ and complexation of $H_2AsO_4^-$ with soluble aluminum in solution and the formation of neutrally charged H_3AsO_4, which depressed the adsorption of As(V) on the alumina surface. The neutrally charged H_3AsO_4 was difficult to adsorb on the NanoActive alumina. However, the fraction (86–100%) of arsenate adsorbed on the NanoActive alumina at pH below 2 was much greater than the fraction (<35%) of $H_2AsO_4^-$

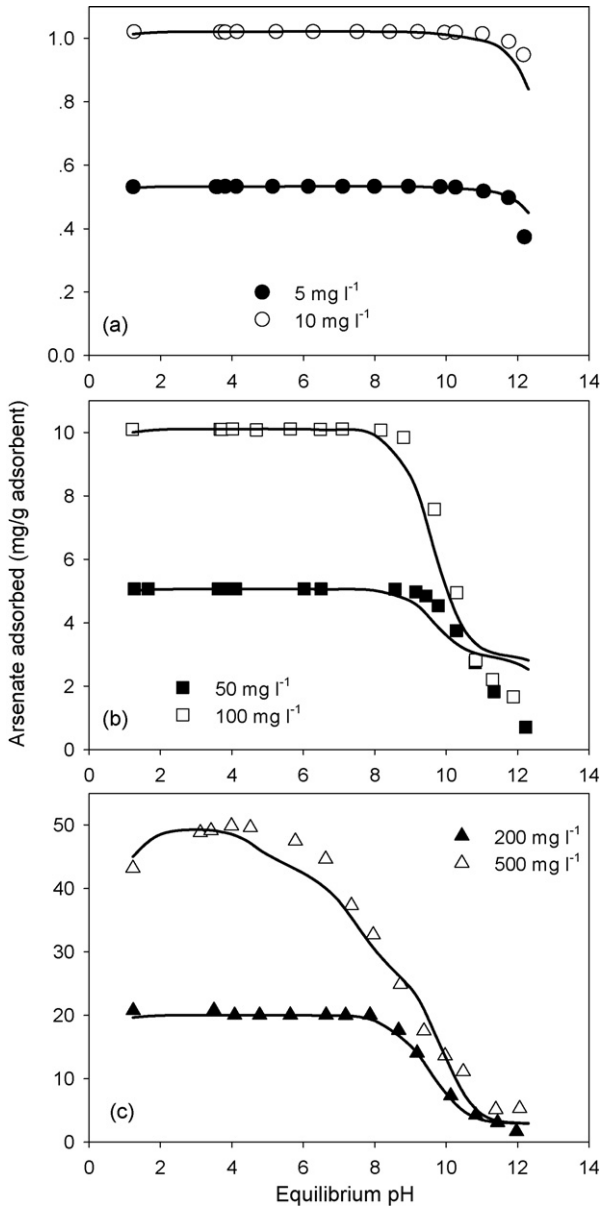

Fig. 3. Comparison of experimental data and model predictions for arsenate adsorption on NanoActive alumina as functions of pH and concentration (concentration of NanoActive alumina: 10 g l^{-1}; arsenate concentration: 5–500 mg g^{-1} as As(V)). Model results are indicated by solid lines.

in solution, which suggests that the adsorption (consumption) of $H_2AsO_4^-$ by NanoActive alumina surface facilitates the transformation of H_3AsO_4 into $H_2AsO_4^-$ on sorbent surface [33]. When the initial arsenate concentration was equal to or less than 200 mg l^{-1}, no reduction in arsenate adsorption was observed at very low pH levels, which may be ascribed to the abundance of surface sites under these conditions. The decrease in adsorption at alkaline pH may be attributed to the increased repulsion between the more negatively charged arsenate species and negatively charged surface sites [34]. In addition, an increase in pH results in a greater proportion of hydroxyl ions in the liquid competing with the adsorbate for the available sites on the surface of NanoActive alumina. This reduces the electrostatic attraction between the adsorbate and adsorbent causing a reduction in adsorption [35]. The strong adsorption of arsenate on NanoActive alumina at pH greater than pH_{PZC} indicated that arsenate was specifically adsorbed on NanoActive alumina [36], but the surface electrostatic effect played an insignificant role in arsenic adsorption.

3.3. FTIR study of adsorbed As species

The symmetry was lowered when As was adsorbed on NanoActive alumina by forming inner sphere complexes, leading to peak splitting or shifting. Fig. 4 shows the spectra of As(V) adsorbed on NanoActive alumina at various pH values and various adsorption densities. The peak positions of the adsorbed samples were significantly different from those of the dissolved As species. The difference was due to symmetry reduction as a result of inner-sphere complex formation. If the symmetry reduction were caused by protonation, as would be the case for outer-sphere adsorption, the bands should exhibit similar positions with regard to the corresponding dissolved As species in the pH range. Therefore, the band shift indicated the formation of inner-sphere complexes. With the similarities of phosphate and arsenate, the band assignment of adsorbed As(V) spectra was comparable to that of $(MO)_2PO_2$ surface complexes having C_{2v} symmetry [37–40]. Because metal ions are not as strongly coordinated to oxygen ions as protons are [37–39,41], the As–OAl bond should be stronger than As–OH. Thus, the uncomplexed As–O bond in $(AlO)_2AsO_2$ should be weaker than that in $(HO)_2AsO_2^-$, and the uncomplexed As–O bond in $(AlO)AsO_3^-$ should be weaker than that in $(HO)AsO_3^{2-}$.

The adsorbed arsenate on NanoActive alumina is characterized by one band at 847–854 cm^{-1}. Goldberg and Johnson [11] observed that the adsorbed arsenate on Al oxide was resolved by a strong band at 850–862 cm^{-1} and they assigned this peak to ν(As–O) vibration of an inner-sphere Al–O–As complex. They declared that the As–O groups were involved in direct complexation to the alumina surface. This difference and the lack of change in band position at various pH values and adsorption densities suggest that As(V) formed same

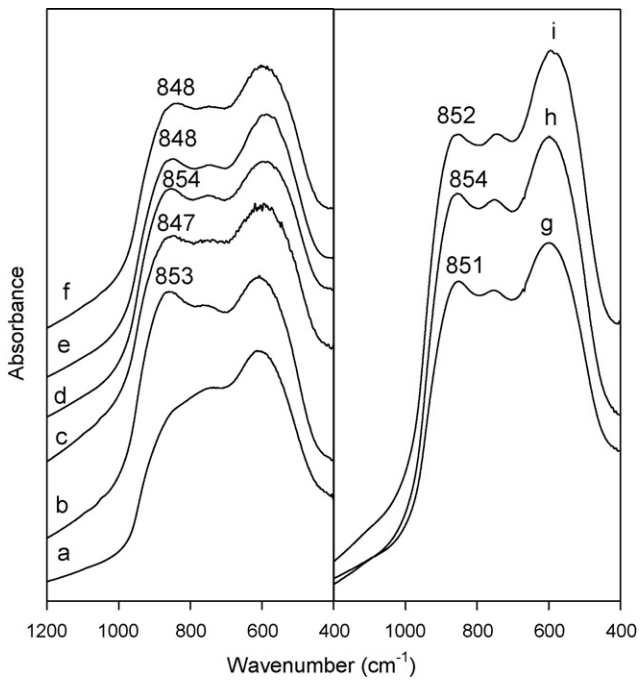

Fig. 4. Diffuse reflectance FTIR spectra of (a) NanoActive alumina and (b–i) NanoActive alumina with adsorbed arsenate at different pH and different adsorption densities: (b) pH 4.4, 72.0 mg g^{-1}; (c) pH 6.3, 54.8 mg g^{-1}; (d) pH 4.4, 99.0 mg g^{-1}; (e) pH 6.0, 81.0 mg g^{-1}; (f) pH 7.5, 54.0 mg g^{-1}; (g) pH 1.33, 65.9 mg g^{-1}; (h) pH 2.66, 83.1 mg g^{-1}; (i) pH 3.32, 104.1 mg g^{-1}.

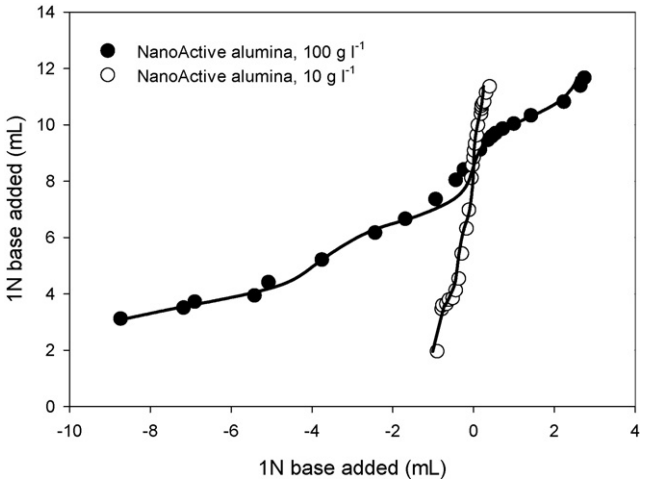

Fig. 5. Titration and curve fitting results for NanoActive alumina (100 ml). Background electrolyte = 0.1 M $NaNO_3$, temperature = 21 °C, equilibration time = 24 h.

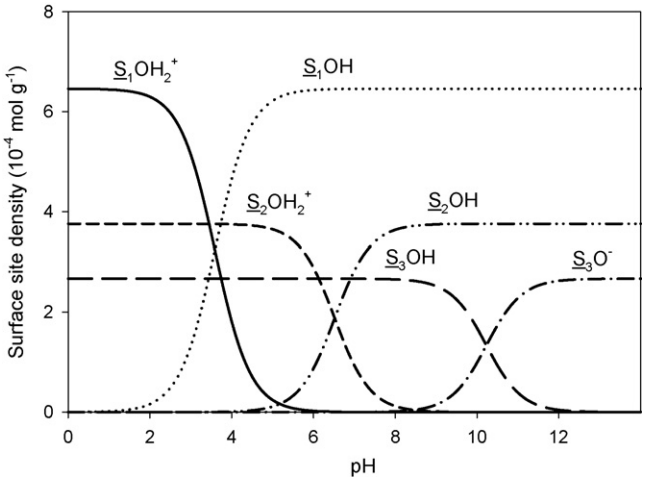

Fig. 6. Surface speciation of NanoActive alumina at different pH.

inner-sphere surface complexes on NanoActive alumina. The peak at 847–854 cm^{-1} can be assigned to the υ(As–O) vibration of a monodentate complex because it appears at a lower frequency than the ν_{as}(As–O) in $HAsO_4^{2-}$. In brief, the FTIR results indicated that arsenate interacted strongly with NanoActive alumina and formed a mono-dentate complex upon adsorption under various pH and adsorption densities.

3.4. Modeling As(V) adsorption data

3.4.1. Surface acidity

The determination of surface acidity is a key step for adsorption modeling [42,43]. Fig. 5 shows the net titration data (open circles and filled circles) of NanoActive alumina suspensions at two different concentrations. The following equation was employed to simulate the net titration data for determining the acid site concentration and the corresponding acidity constant, based on the assumption that multiple types of monoprotic acid sites were present on the particle surface [42]:

$$\Delta V_{SS} = \sum_{i=1-n} \frac{V_0 \underline{S}_{Ti} K_{Hi}}{C} \left(\frac{1}{[H^+] + K_{Hi}} - \frac{1}{[H^+]_0 + K_{Hi}} \right) \quad (1)$$

where ΔV_{SS} is the net volume of the stock acid/base (negative value for acid) solution consumed by the surface acid sites (ml); V_0 is the total volume of the alumina mixture (ml); $\underline{S}_{Ti}$ is the total acid site concentration of the species i (M); K_{Hi} is the acidity constant of the species i (M); C is the concentration of the acid/base stock solution (M); and $[H^+]_0$ is the hydrogen ion concentration of the control unit (M). Note the total surface site concentration $\underline{S}_{Ti} = \Gamma_i \times SS$, where Γ_i is the surface site density for species i (mol g^{-1}) and SS is the solid concentration (g l^{-1}).

The simulation was carried out with a nonlinear regression program, NLREG. The curve fitting results based on the three-site assumption, as indicated by the smooth curves in Fig. 5, best fit the net titration data of NanoActive alumina. Therefore, we hypothesized that there were three types of acid sites, denoted as site $\underline{S}_1$, site $\underline{S}_2$, and site $\underline{S}_3$, on the surface of the NanoActive alumina. The surface site density (Γ) and acidity constant (pK_H) resulting from the modeling process are summarized in Table 1.

Since values of pK_{H1} and pK_{H2} for NanoActive alumina are less than its pH_{zpc}, the protonated surface acid sites $\underline{S}_1$ and $\underline{S}_2$ are positively charged. Similarly, since the pK_{H3} is greater than pH_{zpc}, the deprotonated surface site $\underline{S}_3$ is negatively charged. The protonated surface sites $\underline{S}_1$ and $\underline{S}_2$ could be responsible for adsorbing anionic arsenate species.

3.4.2. Surface speciation

As mentioned before, we hypothesized that the protonated acid surface sites $\underline{S}_1$ and $\underline{S}_2$ are responsible for arsenic adsorption. Since they are positively charged, their deprotonation reactions can be expressed as:

$$\underline{S}_1OH_2^+ = \underline{S}_1OH + H^+ \quad K_{H1} \quad (2)$$

$$\underline{S}_2OH_2^+ = \underline{S}_2OH + H^+ \quad K_{H2} \quad (3)$$

where K_{H1} and K_{H2} are the acidity constants of surface acid sites $\underline{S}_1$, and $\underline{S}_2$, respectively.

The concentrations of the positively charged surface acid sites, $\underline{S}_1OH_2^+$ and $\underline{S}_2OH_2^+$, are expressed as:

$$\underline{S}_1OH_2^+ = \alpha_{1+}\underline{S}_{T1} \qquad \alpha_{1+} = \frac{[H^+]}{[H^+] + K_{H1}} \quad (4)$$

$$\underline{S}_2OH_2^+ = \alpha_{2+}\underline{S}_{T2} \qquad \alpha_{2+} = \frac{[H^+]}{[H^+] + K_{H2}} \quad (5)$$

where $\underline{S}_{T1}$ and $\underline{S}_{T2}$ are the total concentrations (protonated and unprotonated) of site $\underline{S}_1$ and $\underline{S}_2$, respectively; α_{1+} and α_{2+} are the fractions of the protonated surface sites. Fig. 6 demonstrates the surface speciation for all three acid sites at various pH levels.

3.4.3. Modeling As(V) adsorption data with a speciation-based multisite Langmuir isotherm

As the FTIR results indicated that arsenate formed a monodenate complex with NanoActive alumina, the surface electrostatic effects

Table 1
Surface site density and acidity constants of NanoActive alumina.

Sample	Surface site parameters	$\underline{S}_1$	$\underline{S}_2$	$\underline{S}_3$	IEP
NanoActive alumina	Γ (10^{-4} mol g^{-1})	6.22 ± 0.46	3.75 ± 0.22	3.09 ± 0.11	8.0
	pK_H	3.63 ± 0.10	6.52 ± 0.09	10.28 ± 0.08	

Table 2
Parameters obtained through modeling.

Site	$\equiv S_1$		$\equiv S_{2W}$			$\equiv S_{2S}$			R
	$\log K_{S1}$	$\log K_{S2}$	$\log K_{S4}$	$\log K_{S5}$	$\log K_{S6}$	$\log K_{S7}$	$\log K_{S8}$	$\log K_{S9}$	
NanoActive alumina	3.98 ± 0.13	6.33 ± 0.11	5.37 ± 0.12	4.85 ± 0.14	NA	6.18 ± 0.29	7.17 ± 0.35	6.93 ± 0.34	0.471
	3.98 ± 0.13		$\log K_{S2,4,5,6} = 5.82 \pm 0.11$				$\log K_{S7,8,9} = 8.86 \pm 0.24$		0.122

on arsenate adsorption were not considered in our model and the formation of mononuclear (1:1 stoichiometry) surface species was proposed in developing the model [42,44,45]. A model for arsenic adsorption on a single site has been developed by Wang et al. [45]. As discussed above, the protonated surface acid sites $\equiv S_1$ and $\equiv S_2$ on NanoActive alumina were hypothesized to be the surface sites responsible for arsenate adsorption, the multisite model in a system with two different types of sites was as follows:

$$q_{A,tot} = q_{A,1} + q_{A,2} = \frac{q_{max,1} K_{A1} [As(V)]_D}{1 + K_{A1}[As(V)]_D} + \frac{q_{max,2} K_{A2} [As(V)]_D}{1 + K_{A2}[As(V)]_D} \quad (6)$$

where $q_{A,tot}$ = total adsorbed arsenic concentration, $q_{max,1} = \equiv S_{T1}$, $q_{max,2} = \equiv S_{T2}$,

$$K_{A1} = \alpha_{1+}(\alpha_1 K_{S1} + \alpha_2 K_{S2} + \alpha_3 K_{S3})$$

$$K_{A2} = \alpha_{2+}(\alpha_1 K_{S4} + \alpha_2 K_{S5} + \alpha_3 K_{56})$$

K_{S1}, K_{S2} and K_{S3} are adsorption constants of $H_2AsO_4^-$, $HAsO_4^{2-}$, and AsO_4^{3-} on surface acid site $\equiv S_1$, respectively. K_{S4}, K_{S5} and K_{S6} are adsorption constants of $H_2AsO_4^-$, $HAsO_4^{2-}$, and AsO_4^{3-} on surface acid site $\equiv S_2$, respectively. $[As(V)]_D$ is the concentration of arsenate in the solution at equilibrium.

α_1, α_2 and α_3 are fractions of arsenic species $H_2AsO_4^-$, $HAsO_4^{2-}$, and AsO_4^{3-} in solution, respectively.

$$\alpha_1 = \frac{[H^+]^2 K_{a1}}{[H^+]^3 + [H^+]^2 K_{a1} + [H^+] K_{a1} K_{a2} + K_{a1} K_{a2} K_{a3}} \quad (7)$$

$$\alpha_2 = \frac{[H^+] K_{a1} K_{a2}}{[H^+]^3 + [H^+]^2 K_{a1} + [H^+] K_{a1} K_{a2} + K_{a1} K_{a2} K_{a3}} \quad (8)$$

$$\alpha_3 = \frac{K_{a1} K_{a2} K_{a3}}{[H^+]^3 + [H^+]^2 K_{a1} + [H^+] K_{a1} K_{a2} + K_{a1} K_{a2} K_{a3}} \quad (9)$$

where K_{a1}, K_{a2}, K_{a3} are the dissociation constants of arsenic acid.

The modeling results were reasonable, but not ideal, for reflecting the experimental data under alkaline pH conditions. Based on observation of the adsorption data, we hypothesized that the second acid sites, $\equiv S_2$, are composed of two types of arsenic adsorption sites, weak sites ($\equiv S_{2W}$) and strong sites ($\equiv S_{2S}$), following the practice of many researchers [46,47]. Here, it was assumed that a certain percent (R) of surface acid sites S_2 are strong sites. Therefore, the Eq. (6) was modified to be:

$$q_{A,tot} = q_{A,1} + q_{A,2} + q_{A,3} = \frac{q_{max,1} K_{A1} [As(V)]_D}{1 + K_{A1}[As(V)]_D} + \frac{q_{max,2} K_{A2} [As(V)]_D}{1 + K_{A2}[As(V)]_D} + \frac{q_{max,3} K_{A3} [As(V)]_D}{1 + K_{A3}[As(V)]_D} \quad (10)$$

where $q_{max,1} = \equiv S_{T1}$, $q_{max,2} = (1 - R) \times \equiv S_{T2}$, $q_{max,3} = R \times \equiv S_{T2}$, $K_{A3} = \alpha_{2+}(\alpha_1 K_{S7} + \alpha_2 K_{S8} + \alpha_3 K_{S9})$, and K_{S7}, K_{S8} and K_{S9} are the adsorption constants of $H_2AsO_4^-$, $HAsO_4^{2-}$ and AsO_4^{3-} on the strong sites $\equiv S_{2S}$, respectively. R is the ratio of strong sites $\equiv S_{2S}$ to total acid sites $\equiv S_2$ and its value was obtained from modeling. Compared to the original Langmuir isotherm, the Eq. (10) includes the pH effect on the surface site speciation and arsenic speciation, and the competitive effect of different arsenic species for the same surface site.

Theoretically, there should be nine adsorption constants related to the adsorption of three arsenic anion species to three surface sites. In the process of modeling, it was found that adsorption of AsO_4^{3-} on sites $\equiv S_1$ and $\equiv S_{2W}$ was very limited. The limited adsorption of AsO_4^{3-} on sites $\equiv S_1$ may be associated with the fact that no protonated $\equiv S_1$ sites were present when AsO_4^{3-} anions were dominant in the solution. The negligible adsorption of AsO_4^{3-} on sites $\equiv S_{2W}$ may be due to the weak affinity of AsO_4^{3-} for $\equiv S_{2W}$ sites. Therefore, only eight parameters, including seven adsorption constants K_{S1}, K_{S2}, K_{S4}, K_{S5}, K_{S7}, K_{S8}, K_{S9} and R, were used as the adjustable parameters. The values of these parameters were determined by curve fitting with NLREG program and are summarized in Table 2.

The magnitudes of K_{S2}, K_{S4} and K_{S5} were similar, and K_{S7}, K_{S8} and K_{S9} were similar for NanoActive alumina. Although K_{S6} is not important for acid site $\equiv S_{2W}$, in order to simplify the model, we assumed that $K_{S2} = K_{S4} = K_{S5} = K_{S6}$ and $K_{S7} = K_{S8} = K_{S9}$. There are only three empirical adsorption constants in this model, K_{S1}, K_{S4} and K_{S7}. With this idea in mind, the Eq. (10) was further modified to be:

$$q_{A,tot} = \frac{\equiv S_{T1} \alpha_{1+}(\alpha_1 K_{S1} + \alpha_2 K_{S4})[As(V)]_D}{1 + \alpha_{1+}(\alpha_1 K_{S1} + \alpha_2 K_{S4})[As(V)]_D} + \frac{(1 - R) \equiv S_{T2} \alpha_{2+} K_{S4}(\alpha_1 + \alpha_2 + \alpha_3)[As(V)]_D}{1 + \alpha_{2+} K_{S4}(\alpha_1 + \alpha_2 + \alpha_3)[As(V)]_D} + \frac{R \equiv S_{T2} \alpha_{2+} K_{S7}(\alpha_1 + \alpha_2 + \alpha_3)[As(V)]_D}{1 + \alpha_{2+} K_{S7}(\alpha_1 + \alpha_2 + \alpha_3)[As(V)]_D} \quad (11)$$

The values of these three adsorption constants and R were determined with the NLREG program and given in Table 2. This study found that the model with four adjustable parameters could simulate the adsorption data as satisfactorily as that with eight parameters. The ability of the speciation-based model, with only four adjustable parameters to describe arsenate adsorption on NanoActive alumina, is depicted with solid lines in Fig. 3. This model could describe the adsorption data very well over a wide pH range of 1–10 and a wide arsenic concentration range. Since the pK_{a1} of arsenic acid is 2.3 [29], the total fraction of anionic species of arsenic, $\alpha_1 + \alpha_2 + \alpha_3$, is ~1 when pH is greater than 3. As a result, the Equation [11] can be further simplified during practical application when pH is greater than 3:

$$q_{As,tot} = \frac{\equiv S_{T1} \alpha_{1+}(\alpha_1 K_{S1} + \alpha_2 K_{S4})[As(V)]_D}{1 + \alpha_{1+}(\alpha_1 K_{S1} + \alpha_2 K_{S4})[As(V)]_D} + \frac{(1 - R) \equiv S_{T2} \alpha_{2+} K_{S4}[As(V)]_D}{1 + \alpha_{2+} K_{S4}[As(V)]_D} + \frac{R \equiv S_{T2} \alpha_{2+} K_{S7}[As(V)]_D}{1 + \alpha_{2+} K_{S7}[As(V)]_D} \quad (12)$$

Based on the field water pH and arsenic concentration, the total adsorbed arsenic concentration by the sorbent at equilibrium can be calculated using Eq. (12). Therefore, the total bed volumes of water to be treated can be calculated under normal operating conditions. This model can also be conveniently used to predict impacts of sudden pH changes on the treatment performance, avoiding the leaching of adsorbed arsenic to the treated water. Therefore, this model is a useful tool for the design and operation of arsenic treatment systems based on the field water quality condition.

4. Conclusions

The arsenate adsorption envelopes on NanoActive alumina exhibited broad adsorption maxima when the As(V) loading was less than 50 mg g^{-1} sorbent. As the initial As(V) loading increased to 50 mg g^{-1} sorbent, a distinct adsorption maximum was observed at pH 3.2–4.6. FTIR spectra revealed that monodentate complexes were formed upon the adsorption of arsenate on NanoActive alumina over the entire pH range and arsenic loading conditions examined in this study. A speciation-based adsorption model was developed. This model can well describe arsenic adsorption on NanoActive alumina in a broad pH range from 1 to 10, and a wide arsenic loading range from 0.5 to 50 mg g^{-1} adsorbent with only four constants. Modeling results suggested that there are three types of sites on an alumina surface that are responsible for arsenic adsorption. This model offers a substantial improvement and simplification over existing models by simultaneously quantifying the effects of pH and arsenic concentration on arsenic adsorption, and consequently has great field application potential.

Acknowledgements

This work was supported by the Natural Scientific Research Innovation Foundation at Harbin Institute of Technology (HIT.NSRIF.2008.65) and the Development Program for Outstanding Young Teachers at Harbin Institute of Technology (HITQNJS.2007.038).

References

[1] A.K. Dutta, P. Gupta, A. Bandyopadhyay, R.K. Ghosh, S.K. Biswas, Appropriate technology for removal of arsenic from drinking water of rural West Bengal, in: Proceedings of Annual Conference of AWWA, Atlanta, GA, USA, 1997, pp. 15–19.
[2] C. Su, R.W. Puls, Arsenate and arsenite removal by zerovalent iron: kinetics, redox transformation, and implications for in situ groundwater remediation, Environ. Sci. Technol. 35 (2001) 1487–1492.
[3] S.L. Chen, S.R. Dzeng, M.H. Yang, K.H. Chiu, G.M. Shieh, C.M. Wai, Arsenic species in groundwaters of the Blackfoot Disease Area, Taiwan, Environ. Sci. Technol. 28 (1994) 877–881.
[4] V.M. Boddu, K. Abburi, J.L. Talbott, E.D. Smith, R. Haasch, Removal of arsenic(III) and arsenic(V) from aqueous medium using chitosan-coated biosorbent, Water Res. 42 (2008) 633–642.
[5] Y. Zhao, A.I. Zouboulis, K.A. Matis, Removal of molybdate and arsenate from aqueous solutions by flotation, Sep. Sci. Technol. 31 (1996) 769–785.
[6] D. Bhattacharya, A.B. Jumawan Jr., R.B. Grieves, Separation of toxic heavy metals by sulfide precipitation, Sep. Sci. Technol. 14 (1979) 441–452.
[7] J.G. Hering, P.Y. Chen, J.A. Wilkie, M. Elimelech, Arsenic removal from drinking water during coagulation, J. Environ. Eng. 123 (1998) 800–807.
[8] M. Bissen, F.H. Frimmel, Arsenic—a review. Part II: oxidation of arsenic and its removal in water treatment, Acta Hydrochim. Hydrobiol. 31 (2003) 97–107.
[9] S. Goldberg, Chemical modeling of arsenate adsorption on aluminum and iron oxide minerals, Soil Sci. Soc. Am. J. 50 (1986) 1154–1157.
[10] S. Goldberg, Competitive adsorption of arsenate and arsenite on oxides and clay minerals, Soil Sci. Soc. Am. J. 66 (2002) 413–421.
[11] D. Goldberg, C.T. Johnston, Mechanisms of arsenic adsorption on amorphous oxides evaluated using macroscopic measurements, vibrational spectroscopy, and surface complexation modeling, J. Colloid Interf. Sci. 234 (2001) 204–216.
[12] W.E. Halter, H.R. Pfeifer, Arsenic(V) adsorption onto α-Al_2O_3 between 25 and 70 °C, Appl. Geochem. 16 (2001) 793–802.
[13] D.A. Dzombak, F.M.M. Morel, Surface Complexation Modeling: Hydrous Ferric oxide, John Wiley and Sons, New York, 1999.
[14] D.G. Lumsdon, J.C.L. Meeussen, E. Paterson, L.M. Garden, P. Anderson, Use of solid phase characterisation and chemical modeling for assessing the behaviour of arsenic in contaminated soils, Appl. Geochem. 16 (2001) 571–581.
[15] T.H. Hsia, S.L. Lo, C.F. Lin, As(V) adsorption on amorphous iron oxide: triple layer modeling, Chemosphere 25 (1992) 1825–1837.
[16] R.L. Vaughan Jr., B.E. Reed, Modeling As(V) removal by an iron oxide impregnated activated carbon using the surface complexation approach, Water Res. 39 (2005) 1005–1014.
[17] J.A. Wilkie, J.G. Hering, Adsorption of arsenic onto hydrous ferric oxide: effects of adsorbate/adsorbent ratios and co-occurring solutes, Colloid Surface A 107 (1996) 97–110.
[18] J. Antelo, M. Avena, S. Fiol, R. López, F. Arce, Effects of pH and ionic strength on the adsorption of phosphate and arsenate at the goethite–water interface, J. Colloid Interf. Sci. 285 (2005) 476–486.
[19] T. Hiemstra, W.H.V. Riemsdijk, Surface structural ion adsorption modeling of competitive binding of oxyanions by metal (hydr)oxides, J. Colloid Interf. Sci. 210 (1999) 182–193.
[20] R. Weerasooriya, H.J. Tobschall, H.K.D.K. Wijesekara, A. Bandara, Macroscopic and vibration spectroscopic evidence for specific bonding of arsenate on gibbsite, Chemosphere 55 (2004) 1259–1270.
[21] P. Venema, T. Hiemstra, W.H.V. Riemsdijk, Comparison of different site binding models for cation sorption: description of pH dependency, salt dependency, and cation-proton exchange, J. Colloid Interf. Sci. 181 (1996) 45–59.
[22] H.W. Chen, M.M. Frey, D. Clifford, L.S. McNeill, M. Edward, Arsenic treatment considerations, J. Am. Water Works Assoc. 91 (1999) 74–85.
[23] M.M. Frey, J. Chwirk, S. Kommineni, Z. Chowdhury, R. Narasimha, Cost Implications of a Lower Arsenic MCL, AWWA Research Foundation, 2000.
[24] D.A. Clifford, C.C. Lin, Arsenic(III) and Arsenic(V) Removal from Drinking Water in San Ysidro, New Mexico, USEPA Project Summary, Cincinati, OH, USA, 1991.
[25] K.R. Fox, T.J. Sorg, Controlling arsenic, fluoride and uranium by point-of-use treatment, J. Am. Water Works Assoc. 79 (1987) 81–84.
[26] S.W. Hathaway, F.J. Rubel, Removing arsenic from drinking water, J. Am. Water Works Assoc. 79 (1987) 61–65.
[27] W. Driehaus, M. Jekel, U. Hildebrandt, Granular ferric hydroxide—a new adsorbent for the removal of arsenic from natural water, J. Water Supply Res. T. 47 (1998) 30–35.
[28] U. Forstner, I. Haase, Geochemical demobilization of metallic pollutants in solid waste—implications for arsenic in waterworks sludges, J. Geochem. Explor. 62 (1998) 29–36.
[29] X.H. Guan, J.M. Wang, C.C. Chusuei, Removal of arsenic from water using granular ferric hydroxide: macroscopic and microscopic studies, J. Hazard. Mater. 156 (2008) 178–185.
[30] T.F. Lin, J.K. Wu, Adsorption of arsenite and arsenate within activated alumina grains: equilibrium and kinetics, Water Res. 35 (2001) 2049–2057.
[31] X.J. Guo, F.H. Chen, Removal of arsenic by bead cellulose loaded with iron oxyhydroxide from groundwater, Environ. Sci. Technol. 39 (2005) 6808–6818.
[32] H. Genç, J.C. Tjell, D. McConchie, O. Schuiling, Adsorption of arsenate from water using neutralized red mud, J. Colloid Interf. Sci. 264 (2003) 327–334.
[33] S. Mortazavi, F.H. Tezel, A.Y. Tremblay, K. Volchek, Effect of pH on the uptake of arsenic from contaminated water by activated alumina, Adv. Environ. Res. 3 (1999) 103–118.
[34] K.P. Raven, A. Jain, R.H. Loeppert, Arsenite and arsenate adsorption on ferrihydrite: kinetics, equilibrium, and adsorption envelopes, Environ. Sci. Technol. 32 (1998) 344–349.
[35] E. Rosenblum, D. Clifford, The equilibrium capacity of activated alumina, USEPA report EPA/600/2-83-107, 1983.
[36] J.A. Davis, D.B. Kent, Surface complexation modeling in aqueous geochemistry, in: M. Hochella Jr., A.F. White (Eds.), Reviews in Mineralogy, Mineral–Water Interface Geochemistry, vol. 23, Mineralogical Society of America, 1990, pp. 177–260.
[37] M.I. Tejedor-Tejedor, M.A. Aderson, Protonation of phosphate on the surface of goethite as studied by CIR-FTIR and electrophoretic mobility, Langmuir 6 (1990) 602–613.
[38] W. Gong, A real time in situ ATR-FTIR spectroscopic study of linear phosphate adsorption on titania surfaces, Int. J. Miner. Process. 63 (2001) 147–165.
[39] X.H. Guan, Q. Liu, G.H. Chen, C. Shang, Surface complexation of condensed phosphate to aluminum hydroxide: an ATR-FTIR spectroscopic investigation, J. Colloid Interf. Sci. 289 (2005) 319–327.
[40] M. Pena, X.G. Meng, G.P. Korfiatis, C.Y. Jing, Adsorption mechanism of arsenic on nanocrystalline titanium dioxide, Environ. Sci. Technol. 40 (2006) 1257–1262.
[41] S.C.B. Myneni, S.V. Traina, G.A. Waychunas, T.J. Logan, Experimental and theoretical vibrational spectroscopic evaluation of arsenate coordination in aqueous solutions, solids, and at mineral–water interfaces, Geochim. Cosmochim. Acta 62 (1998) 3285–3300.
[42] J. Wang, X. Teng, H. Wang, H. Ban, Characterizing the metal adsorption capability of a class F coal fly ash, Environ. Sci. Technol. 38 (2004) 6710–6715.
[43] C.P. Huang, The surface acidity of hydrous solids, in: M.A. Anderson, A.J. Rubin (Eds.), Adsorption of Inorganics at Solid–Liquid Interfaces, Ann Arbor Science, New York, 1981, pp. 183–217.
[44] C.R. Evanko, D.A. Dzombak, Surface complexation modeling of organic acid sorption to goethite, J. Colloid Interf. Sci. 214 (1999) 189–206.
[45] J. Wang, T. Wang, J.G. Burken, C.C. Chusuei, H. Ban, K. Ladwig, C.P. Huang, Adsorption of arsenic(V) onto fly ash: a speciation-based approach, Chemosphere 72 (2008) 381–388.
[46] M.O. Coppens, A.T. Bell, A.K. Chakraborty, Dynamic, Monte-Carlo and mean-field study of the effect of strong adsorption sites on self-diffusion in zeolites, Chem. Eng. Sci. 54 (1999) 3455–3463.
[47] B.A. Logue, R.W. Smith, J.C. Westall, U(VI) adsorption on natural iron-coated sands: comparison of approaches for modeling adsorption on heterogeneous environmental materials, Appl. Geochem. 19 (2004) 1937–1951.